Structure and properties of protective oleic acid films on magnesium formed upon contact treatment and chamber treatment

A.Yu. Luchkin,* V.A. Luchkina, I.A. Kuznetsov, A.A. Chirkunov, O.A. Goncharova, Yu.I. Kuznetsov, S.S. Vesely and N.N. Andreev

A.N. Frumkin Institute of Physical Chemistry and Electrochemistry, Russian Academy of Sciences, Leninsky pr. 31, 119071 Moscow, Russian Federation
**E-mail: andreyluchkin23@gmail.com*

Abstract

The structure and properties of protective layers formed by oleic acid (OA) upon contact and chamber treatment of magnesium have been studied by a set of corrosion, electrochemical and physical methods. It has been found that treatment of magnesium in an OA solution in isopropyl alcohol and in hot OA vapors (chamber treatment, CT) results in an increase in metal corrosion resistance and inhibition of its anodic dissolution. CT is more efficient than contact treatment. In both variants of magnesium treatment, OA forms protective surface films with approximately the same thickness, which however have different structures. When magnesium is immersed in an OA solution, rounded agglomerates almost merging with each other are formed on its surface. In the case of CT, the surface films have a reticulated structure. The protective effect of OA is associated with magnesium passivation. However, in the case of CT, passive films are characterized by larger pitting potentials and anti-pitting basis in chloride-containing electrolytes. Both variants of magnesium corrosion inhibition are characterized by a mixed blocking–activation mechanism. The activation mechanism predominates in the case of CT.

Received: October 18, 2023. Published: October 26, 2023 doi: 10.17675/2305-6894-2023-12-4-16

Keywords: *magnesium, oleic acid, gas-steam treatment, corrosion inhibitor, AFM, EIS.*

1. Introduction

Due to the intensification of the use of magnesium and its alloys in various industries, ways to improve their corrosion resistance under atmospheric conditions have been actively searched for in recent years [1–6]. Organic inhibitors are widely used to protect metal items from atmospheric corrosion in various circumstances, including transportation and storage [7–12]. The action of organic inhibitors is associated with the formation of thin surface films on a metal.

There are two main types of atmospheric corrosion inhibitors:

– contact inhibitors applied in the form of an active substance or solutions directly onto the surface to be protected. Preservation with these inhibitors is often performed by immersion [13–20];
– vapor-phase inhibitors that reach the metal surface as vapors at ambient temperature (volatile inhibitors) or upon heating (chamber inhibitors, CIN).

Compounds with high vapor pressure are used as volatile inhibitors. Their use is reasonable where it is possible to seal the volume to be protected for the entire preservation period. As volatile inhibitors vaporize at ambient temperature, they saturate the volume inside the package, reach the metal as vapors and adsorb on it to form protective layers. Many studies deal with the theoretical and practical aspects of their action [21–23]. They can protect both ferrous and non-ferrous metals. However, it should be stated that there are no efficient volatile corrosion inhibitors for magnesium on the market of the temporary protection of metals.

The use of CIN is a new vapor-phase protection approach. The preservation of metals with these agents (chamber treatment, CT) involves a short-term exposure of a metal in special chambers to the vapors of inhibitors that are low-volatile under ordinary conditions, but at elevated temperatures where their volatility increases manifold. This treatment creates protective adsorption films on a metal, which remain stable after the metal is removed from the chamber. This method allows one to obtain protective films on magnesium-based materials [24].

Obviously, low-volatile organic compounds such as oleic acid (OA) can be used both as contact inhibitors and as CINs [25, 26]. At the same time, the structure and properties of protective layers of the same inhibitor obtained by the vapor-phase and contact methods have not been compared previously. Such a comparison for the protection of magnesium with OA was the purpose of this work.

2. Materials and Methods

2.1. Materials

The studies were performed using samples of Mg90 magnesium [27] with the composition indicated in Table 1.

Table 1. Chemical composition of Mg90 (mass%).

Mg	Fe	Si	Ni	Cu	Al	Mn	Zn	Pb	Sn
99.95	0.003	0.004	0.001	0.003	0.01	0.01	0.01	0.005	0.005

All the reagents used in this work were of “pure” or “chemically pure” grades.

2.2. Preparation and passivation of samples

Magnesium plates with dimensions of 30×25×5 mm were used for the corrosion studies. Before the treatment, they were polished with grinding papers with P240–P1500 grain size and then degreased with acetone.

Rectangular metal plates with dimensions of 10×10×1 mm served as the samples for atomic force microscopy. After grinding, they were sequentially polished with ACM diamond pastes with particle sizes from 20 to 0.1 μm. The final polishing was performed using the OPS liquid (Germany) containing 0.05 μm colloidal SiO_2 particles.

Ellipsometric studies were performed on magnesium plates with dimensions of 30×20×4 mm. The surface preparation of the samples was similar to that used for atomic force microscopy.

Voltammetric and impedance studies were performed using cylindrical electrodes embedded in epoxy resin shells. The lower end of each cylinder served as the working surface. Its area was 0.5 cm^2. The surface preparation before application of OA films was similar to that used in the corrosion experiments.

Contact protection of magnesium was performed by immersing samples and electrodes into solutions of OA in isopropyl alcohol (IPA) stirred with a magnetic stirrer.

Vapor phase protection was carried out in a sealed chamber with a volume of 0.6 L containing 0.5 g OA. The chamber was placed in a desiccator preheated to the required temperature.

The modes (solution concentrations, duration and temperature) used for magnesium treatment with the inhibitor are described below in the article.

2.3. Accelerated corrosion tests

The protective aftereffect (PAE) of the resulting films was estimated under 100% relative air humidity and recurrent moisture condensation conditions. The samples were suspended on polymer hooks to the lids of airtight glass cells in such a way that they did not come into contact with each other and with the cell walls. The cell volume was 0.6 liters. Hot (50°C) water (0.15 L) was poured on the bottom of each cell, which caused abundant condensation of moisture on the samples. After that, the cells were placed in a thermostatically controlled SNOL 50/350 cabinet, where the following temperature conditions were maintained: 8 h – 40°C, 16 h – 20°C. The samples were examined once every 30 min without opening the cells. During the tests, the time to the formation of corrosion sites on magnesium (τ_{prot}) was recorded.

2.4. Atomic force microscopy

The surface topography was measured in open air using a SolverNext II atomic force microscope manufactured by NovaPhotonix LLC (Russia) in amplitude modulation mode. A silicon probe with a conductive platinum coating, a resonance frequency of 73 kHz, and an elasticity coefficient of 4.5 N/m was used.

2.5. Ellipsometry

The thicknesses of films (*d*) formed on magnesium were measured with a manual Gartner ellipsometer with light beam modulation and with advanced recording of light emission. The radiation source was a diode-pumped solid-state laser, model LSM-S-111-10-NNP25, with a wavelength of 540 nm. The accuracy in determining the angles of the polarizer and analyzer was ±0.05°. The angles Δ and Ψ were determined according to the zero scheme, *i.e.*, by alternately rotating the polarizer and analyzer to achieve the minimum intensity on the measuring device. The values of Δ and Ψ were calculated from the angular values of the polarizer and analyzer at the minimum intensity. Film thicknesses were calculated using the Elipsometry Calculation Spread Sheet program (E. Kondoh) [28]. The variation in ellipsometric angles Δ and Ψ was used to describe the experimental data:

$$\delta\Delta = \Delta - \Delta_0 \quad (1)$$

and

$$\delta\Psi = \Psi - \Psi_0 \quad (2)$$

where Δ_0 and Ψ_0 correspond to the initial surface state.

2.6. Voltammetric tests

An IPC-pro potentiostat (Russia) and a standard three-electrode cell with divided electrode spaces were used. A platinum wire served as the auxiliary electrode. The potentials (*E*) were measured *versus* a saturated silver chloride electrode and converted to the normal hydrogen scale. Experiments were performed in an aqueous solution containing 0.05 M NaCl. The electrodes were placed in a cell with the electrolyte, kept for 5 min, and polarized anodically from the established potential (E_0) at a sweep rate of 0.2 mV/s. The protective properties of the films were estimated by the pitting potentials (E_{pt}) and the anti-pitting basis:

$$\Delta E = E_{pt} - E_0 \quad (3)$$

2.7. Electrochemical impedance spectroscopy

Electrochemical impedance spectra were obtained using an IPC-pro potentiostat and an FRA frequency response analyzer (Russia). The experiments were carried out in a cell, on electrodes, and under conditions similar to those used in the voltammetric tests. The frequency was varied within 0.1 to 100,000 Hz. The electrochemical impedance parameters were calculated using the equivalent circuit (Figure 1) widely used for various metals and alloys [10, 24, 29, 30]:

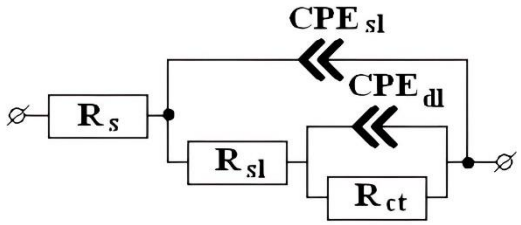

Figure 1. Equivalent circuit used to describe electrochemical impedance data.

In this scheme, R_s is the resistance of the bulk electrolyte between the auxiliary and working electrodes that does not affect the electrode processes and depends on the conductivity of the medium and the cell geometry; R_{sl} is the resistance of oxide-hydroxide and adsorption surface layers; R_{ct} is the polarization resistance characterizing the electrochemical kinetics of the corrosion process; CPE_{sl} is the constant phase element characterizing the capacitance of the surface oxide and/or adsorption layers; and CPE_{dl} is the constant phase element reflecting the capacitance of the double electric layer. The impedance of the constant phase element was described by the equation:

$$z_{CPE} = A^{-1}\left(j\omega\right)^{-n} \quad (4)$$

where A is the proportionality coefficient; j is the imaginary unit; ω is the complex frequency related to the alternate current frequency; and n is the exponent that designates the phase deviation, $0 \le \left| n \right| \le 1$.

Processing of the results and calculation of the parameters of the equivalent circuit were carried out using the Dummy Circuits Solver program, version 2.1 [28]. The calculated data matched the experimental ones by no less than 98%.

The degree of protection of a steel electrode was calculated using the formula:

$$Z = \left(R^{inh} - R^{bg}\right) \Big/ R^{inh} \cdot 100 \quad (5)$$

where R^{bg} and R^{inh} are the total resistances of metal-electrolyte interface interaction, which includes R_{ct} and R_{sl}, before and after electrode treatment, respectively.

3. Results and Discussion

3.1. Accelerated corrosion tests

At the first stage of the tests, the optimum conditions of OA film formation (in terms of protective properties) were determined for both treatment methods. The OA concentration and treatment time[1] were the key factors of magnesium passivation in solutions, or else the time and temperature in the case of CT.

[1] Since isopropanol is a highly inflammable fluid, no tests were performed at elevated temperatures.

To determine the optimum concentration of the OA solution in IPA, the metal was treated for 1 h in solutions containing 2, 4, 8, 16, 32, or 64 mM of the inhibitor. The results of corrosion tests are presented in Table 2.

Table 2. PAE of adsorption films formed on treatment of magnesium in OA solutions with various concentrations. The treatment time was 1 hour.

OA concentration, mM	**0**	**2**	**4**	**8**	**16**	**32**	**64**
τ_{prot}, h	0.5	22.5	22.5	40	36	22.5	22.5

In the humid atmosphere, magnesium in the initial state (IS) and that treated for 1 h in pure IPA (treatment conditions A) already began to corrode after 0.5 h of the tests. The surface of the alloy tarnished and extensive black spots appeared on it.

Treatment in OA solution delayed corrosion initiation. It may be due to the formation of protective layers of OA itself and/or its magnesium salts.

As the OA concentration was increased from 2 to 8 mM, the corrosion resistance of the metal also increased. At 8 mM, the τ_{prot} became 40 hours. When we were planning this experiment, we expected to determine the OA concentration above which the protective properties would increase only slightly. However, as the OA concentration was increased above 8 mM, the protective effect not only failed to increase but even decreased. It is worth noting that when the samples were treated in solutions with concentrations of 16 mM or higher, nonuniform coatings with OA droplets visible to the naked eye were formed on them. Probably, the decrease in protection is due to the dissolution of protective films of magnesium oleates therein.

In the second series of experiments, the duration of immersion of samples in the solution with the optimal inhibitor concentration (8 mM) was varied. The data in Table 3 show that with an increase in the treatment time, the protective properties of OA first increased and then stabilized after 60 min. Thus, the optimal time for the formation of a protective film in the alcohol solution was 60 min. It should be noted that no OA droplets were formed on the surface when the samples were kept in the OA solution with the optimum concentration, regardless of the treatment time.

Table 3. PAE of adsorption films formed upon magnesium treatment in 8 mM OA solution for various periods of time.

Treatment time, min	**0**	**5**	**15**	**30**	**60**	**90**	**120**
τ_{prot}, h	0.5	8	16	30	40	40	40

Thus, the optimum conditions of magnesium treatment using OA solutions in IPA are: a concentration of 8 mM and a duration of 60 min (conditions B).

In the case of the chamber protection of metals, the CT temperature and time are the critical parameters [24, 25, 31]. Thermal treatment (TT) of magnesium itself, regardless of

its duration, did not affect the corrosion resistance of the metal. At treatment temperatures up to 100°C, the metal surface tarnished already after 0.5 h of exposure to the corrosive conditions. At treatment temperatures above 100°C (including 140°C, 15 min, *i.e.*, conditions C), the value of τ_{prot} remained the same. However, the character of corrosion changed, namely, the corrosion damage had the form of black spots.

One-hour exposure of magnesium in a cell with a certain amount of OA at room temperature did not increase the corrosion resistance of the metal (Table 4). An increase in the temperature to 40–80°C led to a 6–8 fold increase in τ_{prot}. An even greater growth of the protective properties of OA was observed in the CT temperature range of 100–120°C. The maximum PAE was observed at 140°C. Treatment of samples at higher temperatures did not increase the protective effect of the surface films. At the same time, after CT for 1 h at 140°C, a matte film resistant to mechanical impact could be seen with naked eye on the metal surface. It may be assumed that this film is a result of OA polymerization. If the temperature was increased to 150°C, the surface film became inhomogeneous.

Table 4. Results of accelerated corrosion tests of magnesium after CT with OA at various temperatures. The treatment time was 1 h.

CT temperature, °C	**25**	**40**	**60**	**80**	**100**	**120**	**140**	**150**
τ_{prot}, h	0.5	3.0	4.0	4.0	12.0	24.0	42.0	40.0

A search for the optimum treatment time showed that the maximum corrosion resistance of magnesium was achieved upon CT for 15 min (Table 5). The appearance of the metal surface did not change after that time, which indicates that the thickness of OA films was relatively small. Prolonged (3 h or more) CT of samples in OA vapors favored the formation of a thick inhomogeneous brown surface layer on the surface. We failed to estimate the time of full protection provided by this coating due to its coloration that "masked" the corrosion sites.

Table 5. Results of accelerated corrosion tests of magnesium after CT with OA for various periods of time. The treatment temperature was 140°C.

CT duration, min	**5**	**15**	**30**	**60**	**90**	**180**	**300**
τ_{prot}, h	24	120	96	42	36	–	–

Thus, the optimum conditions of magnesium CT with OA are: temperature 140°C, duration 15 min (conditions D).

The designations of magnesium treatment conditions that are introduced above and will be used below in the description of experimental data are summarized in Table 6.

Table 6. Designations of magnesium treatment conditions.

Designation	Treatment conditions
IS	Initial state
A	1 h in IPA without the inhibitor (background for contact protection)
B	1 h in 8 mM solution of OA in IPA (optimum conditions for contact protection)
C	TT for 15 min at 140°C without OA (background for CT)
D	CT for 15 min at 140°C with OA (optimum conditions for CT)

Comparison of the two corrosion inhibition methods under optimum conditions indicates that CT of magnesium with OA provides metal protection for a longer time.

Information on the structure of OA films formed by different methods is provided by atomic force microscopy.

3.2. Atomic force microscopy

The images of the surfaces taken before and after various treatments are presented in Figure 2. The image of the magnesium surface in the initial state shows polishing scratches as well as grains up to 17 nm high. The surface roughness was 7±1 nm.

One-hour treatment of magnesium in IPA nearly did not change the surface appearance.

Treatment of magnesium under conditions B resulted in the formation of rounded agglomerates with an average size of 100–150 nm on the surface. They favored an increase in the surface roughness of the sample (10±2 nm). These structures covered the defects of sample preparation: neither scratches nor grains were visible in the image.

The surface appearance of the samples after the TT (conditions C) did not change considerably in comparison with the IS.

Chamber treatment of magnesium under optimal conditions led to OA deposition in the form of a light brown layer. It was sufficiently stable and did not undergo deformation under a weak mechanical impact. As it can be seen in Figure 2D, the coating formed on the sample surface had a reticulated structure with slightly nonuniform thickness. This film "masked" the substrate relief completely.

Thus, contact and vapor-phase treatment of magnesium with OA under optimal conditions leads to the formation of layers with different structures on the surface.

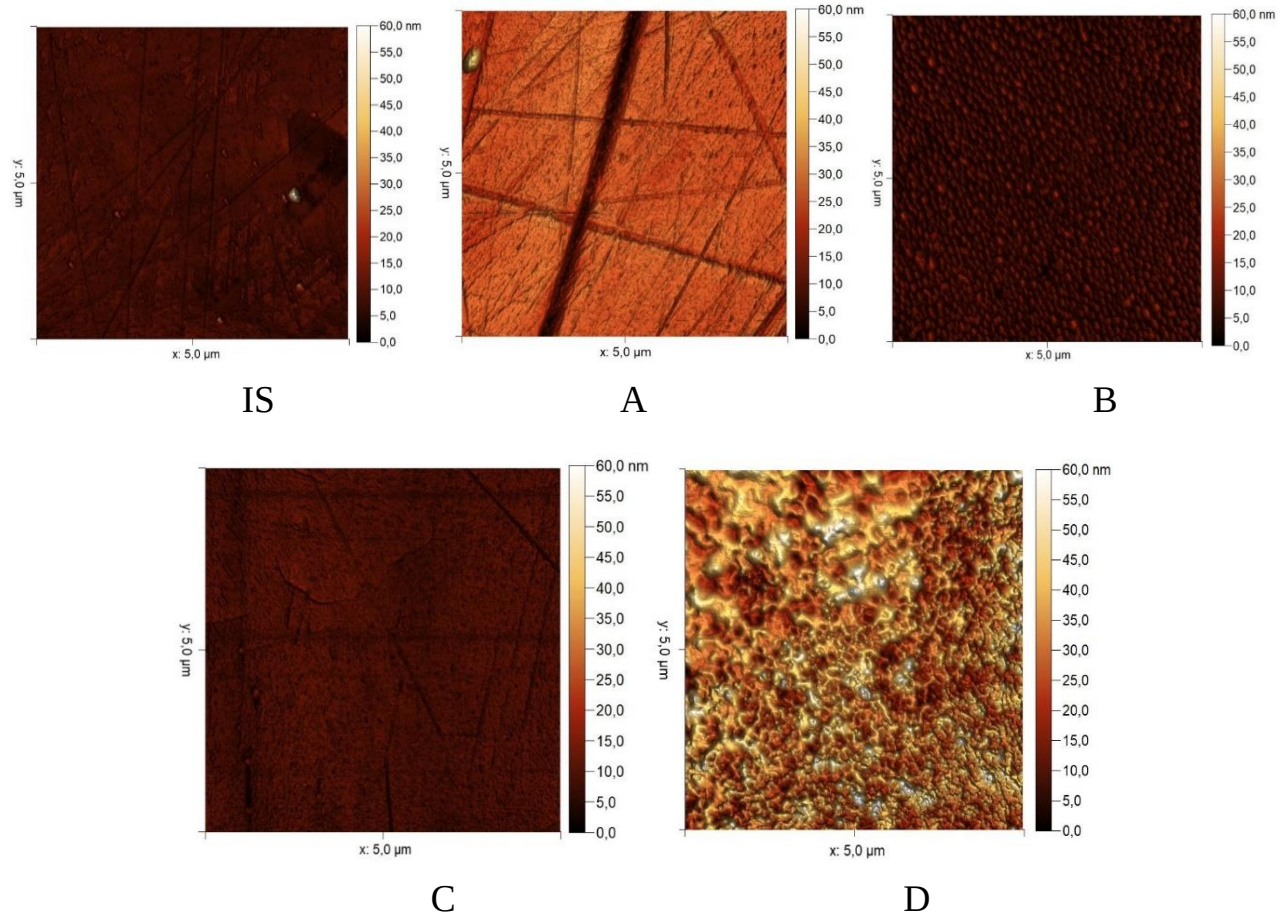

Figure 2. Surface topography of a magnesium sample in the IS after treatment under conditions A, B, C, and D.

3.3. Ellipsometry

The thicknesses of OA surface layers formed at the optimal parameters of contact and vapor phase protection of magnesium (conditions B and D) were estimated using the reflectance ellipsometry method. In both cases, a film with a thickness of about 65 nm was formed on the surface. This fact indicates that in these experiments, the coating thickness is not the factor that determines the protective properties.

3.4. Voltammetric tests

The results of voltammetric tests are presented in Figure 3 and in Table 7.

Once magnesium in the IS was immersed into the electrolyte, it acquired the potential $E_0 = -1.405$ V. Upon anodic polarization of the electrode, the current density of metal dissolution increased sharply, which is characteristic of active metal dissolution. The surface of the electrodes after they were removed from the electrolyte at the end of polarization was matted. The polarization curves of magnesium treated under conditions A and C almost repeated the curves of the electrode in the IS, which is consistent with the

results of corrosion tests where treatment under these conditions did not affect the corrosion resistance of magnesium.

The treatment of magnesium with the OA solution under conditions B enriched E_0 by 0.03 V. A passive region 0.065 V long appeared on the curve. At $E = -1.305$ V, the current density increased sharply. The surface of the electrodes after the tests retained a metallic luster, but black dots, *i.e.*, places where film breakdown occurred, were noticeable on it.

Chamber treatment of an electrode in OA under conditions D suppressed the anodic process most strongly. The passive range expanded noticeably. The E_{pit} values increased to −1.28 V.

Thus, polarization measurements indicate that magnesium is passivated with OA after treatment by both variants. The chamber method of metal treatment is noticeably more efficient in suppressing its anodic dissolution than the contact method.

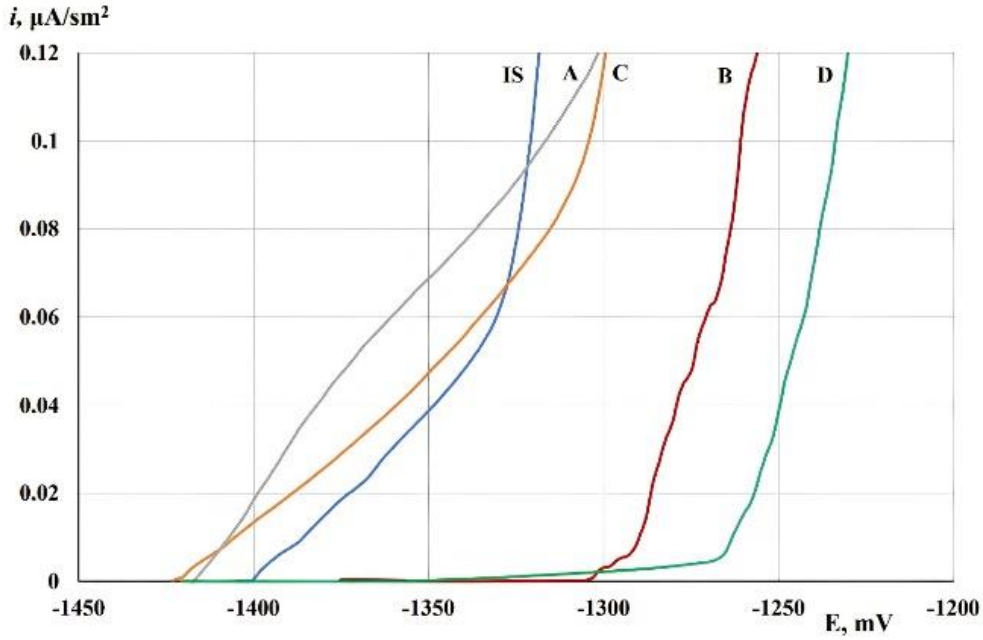

Figure 3. Anodic polarization curves of magnesium in 0.05 M NaCl solution. IS and treatment under conditions A, B, C, and D.

Table 7. Characteristics of anodic polarization curves of electrodes treated under various conditions. 0.05 M NaCl solution.

Treatment conditions	E_0, V	E_{pit}, V	ΔE
IS	−1.405	−1.405	0
A	−1.420	–	–
B	−1.370	−1.305	0.065
C	−1.425	–	–
D	−1.420	−1.280	0.140

3.5. Electrochemical impedance spectroscopy

This method allows one to get more information concerning the effect of films on the corrosion process and determine the mechanism of inhibitor's action.

The electrochemical impedance spectrum of the magnesium electrode in the IS is shown in Figure 4. The Nyquist plot of such a sample has the shape of a distorted half-circle with two pronounced capacitive loops. The first one, which is located in the high- and medium-frequency regions, refers to the surface oxide-hydroxide layers. The second one with a smaller radius is localized in the low-frequency region. It characterizes the processes that occur in the double layer. According to the results simulation using the equivalent circuit shown in Figure 1 (Table 8), the main contribution to the charge transfer resistance across the metal–solution interface is made by the surface oxide-hydroxide film: the value of R_{sl} is 2 times higher than R_{ct}. The value of n_{sl} indicates the homogeneity of the oxide-hydroxide film, and that of n_{dl} shows that the electrode processes in the double layer are practically not complicated by diffusion. The absolute values of CPE_{sl} and CPE_{dl} characterize the initial state of the magnesium surface and serve, along with the values of R_{sl} and R_{ct}, as a starting point for estimating the changes in its properties after metal treatment by various methods.

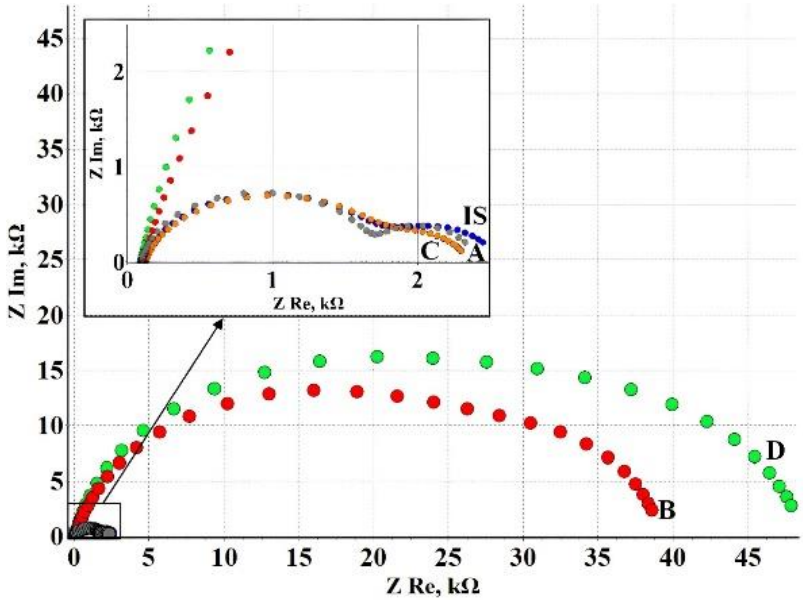

Figure 4. Nyquist plots of magnesium in 0.05 M NaCl solution. IS and treatment under conditions A, B, C, and D.

Treatment of the electrode under conditions A and C had almost no effect on the shape and radius of the AC plots. The insignificant deviation of these values from the corresponding values for the IS was within the scatter of data in parallel experiments.

Table 8. Equivalent circuit parameters after treatment of magnesium electrode under various conditions. 0.05 M NaCl solution.

Treatment conditions	R_s, kOhm	CPE_{sl}, S·s^n	n_{sl}	R_{sl}, kOhm	CPE_{dl}, S·s^n	n_{dl}	R_{ct}, kOhm	Z %
IS	0.10	$8.72\cdot10^{-6}$	0.88	1.69	$5.90\cdot10^{-4}$	0.85	0.75	–
A	0.10	$7.55\cdot10^{-6}$	0.92	1.64	$7.40\cdot10^{-4}$	1.00	0.65	−6.65
B	0.10	$1.51\cdot10^{-6}$	0.88	31.34	$2.40\cdot10^{-5}$	1.00	7.66	93.75
C	0.10	$9.71\cdot10^{-6}$	0.86	1.72	$5.80\cdot10^{-4}$	0.86	0.50	−9.71
D	0.10	$9.78\cdot10^{-7}$	0.91	22.12	$1.19\cdot10^{-5}$	0.87	26.45	94.98

Magnesium treatment under conditions B resulted in an 18.5-fold increase in R_{sl} and a 10-fold increase in R_{ct}. At the same time, CPE_{sl} and CPE_{dl} decreased significantly, *i.e.*, 5.8- and 25-fold, respectively. The values of n_{sl} and n_{dl} show that the constant phase elements of the film and of the double layer behave as pure capacitance. In turn, the decrease in the double layer capacitance is due to a decrease in the electrochemically active surface. The Z value is 93.75%.

CT of magnesium in OA vapors (conditions D) increased the hodograph radius and the values of R_{sl} and R_{ct} significantly (13- and 35-fold, respectively). The values of CPE_{sl} and CPE_{dl} also decreased more significantly than for the electrode after contact treatment at the optimum concentration. Comparison of the change in the electrochemically active surface area based on the CPE_{dl} values shows that it decreased almost 2 times more strongly after CT. This is probably due to the larger value of R_{ct}. The values of n_{sl} and n_{dl} are equal or close to 1, indicating the homogeneity of the films and the absence of diffusion in the double layer. The Z value increased to 94.98%

The results of data simulation using the equivalent circuit make it possible to numerically estimate the contribution of different mechanisms that provide the inhibitory effect of OA and to determine the partial coefficients of corrosion inhibition.

Two main mechanisms of action of adsorption-type corrosion inhibitors, the blocking and activation ones, are known [32]. In the first case, the adsorbing inhibitor blocks a fraction of the metal surface, thus reducing the corrosion rate, but does not affect the kinetics of electrode processes on the remaining non-blocked surface. In contrast, the activation mechanism implies that corrosion inhibition occurs due to changing the activation energy of the corrosion processes and hence their kinetics. Both mechanisms are usually realized simultaneously, but their contributions to the inhibitory effect may differ.

The R_{sl} value in the equivalent scheme that we used reflects the effect of the surface layer, therefore it can serve as a criterion for estimating the blocking effect of the inhibitor. The corrosion inhibition coefficient due to surface blocking (γ_{bl}) is the ratio of R_{sl} resistance of the sample after treatment with the inhibitor to the R_{sl} of the sample without inhibitor treatment:

$$\gamma_{bl} = R_{sl}^{inh} / R_{sl}^{bg} \quad (6)$$

Using a similar approach, the effect of OA on the Faraday corrosion process can be judged by the value of the R_{ct} element. The coefficient of electrochemical reaction inhibition due to the inhibitor (γ_{act}) can be determined as the ratio of the charge transfer resistances R_{ct} for the inhibited and uninhibited samples:

$$\gamma_{act} = R_{ct}^{inh} / R_{ct}^{bg} \quad (7)$$

The degrees of protection of Mg90 with OA films of various origin on various substrates by the blocking and activation mechanisms are presented in Table 8.

Table 8. Coefficients of corrosion inhibition by the activation and blocking mechanisms under optimum conditions of magnesium treatment.

Treatment conditions	γ_{bl}	γ_{act}
B	11.18	10.26
D	13.07	35.46

After contact treatment of magnesium, the γ_{bl} value reached 11.18, while γ_{act} was 10.26, which allows us to state that the inhibitor acts by a mixed mechanism with predominance of the blocking mechanism. In the case of CT, γ_{act} is larger than γ_{bl} nearly by a factor of 3, which indicates that the activation mechanism predominates.

4. Conclusions

1. Treatment of magnesium in OA solutions in IPA and in hot vapors of OA increases the corrosion resistance of the metal and hinders its anodic dissolution. CT is more efficient than contact treatment.
2. In both variants of magnesium treatment, OA forms protective surface films with nearly the same thickness but with different structures. When magnesium is immersed in an OA solution, almost merged round agglomerates are formed on the surface. In the case of CT, the surface films have a reticulated structure.
3. The protective effect of OA is caused by magnesium passivation. However, the passive films formed upon CT are characterized by high values of the pitting potential and anti-pitting basis in chloride-containing electrolytes.
4. Both variants of magnesium corrosion inhibition are characterized by a mixed blocking-activation mechanism. In the case of CT, the activation mechanism predominates.

5. Funding Sources

This study was financially supported by the Russian Science Foundation (Grant no. 23-23-00092 “Development of scientific principles of the self-organization of protective

nanoscale films of organic inhibitors on the surface of metals and alloys from the vapor-gas phase").

References

1. M. Esmaily, J.E. Svensson, S. Fajardo, N. Birbilis, G.S. Frankel, S. Virtanen, R. Arrabal, S. Thomas and L.G. Johansson, Fundamentals and advances in magnesium alloy corrosion, *Prog. Mater. Sci*., 2017, **89**, 92–193. doi: 10.1016/j.pmatsci.2017.04.011
2. A. Atrens, Zh. Shi, S.U. Mehreen, S. Johnston, G.-L. Song, X. Chen and F. Pan, Review of Mg alloy corrosion rates, *J. of Magnesium Alloys*, 2020, **8**, 989–998. doi: 10.1016/j.jma.2020.08.002
3. A.S. Gnedenkov, V.S. Filonina, S.L. Sinebryukhov and S.V. Gnedenkov, A Superior Corrosion Protection of Mg Alloy via Smart Nontoxic Hybrid Inhibitor-Containing Coatings, *Molecules*, 2023, **28**, 2538. doi: 10.3390/molecules28062538
4. B. Li, Z. Zhang, T. Liu, Z. Qiu, Y. Su, J. Zhang, C. Lin and L. Wang, Recent Progress in Functionalized Coatings for Corrosion Protection of Magnesium Alloys—A Review, *Materials*, 2022, **15**, 3912. doi: 10.3390/ma15113912
5. B. Vaghefinazari, E. Wierzbicka, P. Visser, R. Posner, R. Arrabal, E. Matykina, M. Mohedano, C. Blawert, M.L. Zheludkevich and S.V. Lamaka, Chromate-Free Corrosion Protection Strategies for Magnesium Alloys—A Review: Part III—Corrosion Inhibitors and Combining Them with Other Protection Strategies, *Materials*, 2022, **15**, 8489. doi: 10.3390/ma15238489
6. N.A. Johari, J. Alias, A. Zanurin, N.S. Mohamed, N.A. Alang and M.Z.M. Zain, Anti-corrosive coatings of magnesium: A review, *Mater. Today: Proc*., 2022, **48**, 1842–1848. doi: 10.1016/j.matpr.2021.09.192
7. X. Lu, Y. Li, P. Ju, Y. Chen, J. Yang, K. Qian, T. Zhang and F. Wang, Unveiling the inhibition mechanism of an effective inhibitor for AZ91 Mg alloy, *Corros. Sci*., 2019, **148**, 264–271. doi: 10.1016/j.corsci.2018.12.025
8. Y. Qiu, X. Tu, X. Lu and J. Yang, A novel insight into synergistic corrosion inhibition of fluoride and DL-malate as a green hybrid inhibitor for magnesium alloy, Corros. Sci., 2022, **199**, 110177. doi: 10.1016/j.corsci.2022.110177
9. S.V. Lamaka, B. Vaghefinazari, D. Mei, R.P. Petrauskas, D. Höche and M.L. Zheludkevich, Comprehensive screening of Mg corrosion inhibitors, *Corros. Sci*., 2017, **128**, 224–240. doi: 10.1016/j.corsci.2017.07.011
10. Y. Li, Xi. Lu, D. Mei, T. Zhang and F. Wang, Passivation of corrosion product layer on AM50 Mg by corrosion inhibitor, *J. Magnesium Alloys*, 2022, **10**, 2563–2573. doi: 10.1016/j.jma.2021.11.020
11. T. Zhao, Zh. Wang, Y. Feng and Q. Li, Synergistic corrosion inhibition of sodium phosphate and sodium dodecyl sulphate on magnesium alloy AZ91 in 3.5 wt% NaCl solution, *Mater. Today Commun*., 2022, **31**, 103568. doi: 10.1016/j.mtcomm.2022.103568

12. A. Frignani, V. Grassi, F. Zanotto and F. Zucchi, Inhibition of AZ31 Mg alloy corrosion by anionic surfactants, *Corros. Sci*., 2012, **63**, 29–39. doi: 10.1016/j.corsci.2012.05.012
13. K.A. Yasakau, A. Maltseva, S.V. Lamaka, D. Mei, H. Orvi, P. Volovitch, M.G.S. Ferreira and M.L. Zheludkevich, The effect of carboxylate compounds on Volta potential and corrosion inhibition of Mg containing different levels of iron, *Corros. Sci*., 2022, **194**, 109937. doi: 10.1016/j.corsci.2021.109937
14. D.J.J. Jebaraj, N.R.J. Hynes and N.K. Basanth, Corrosion Inhibition in Magnesium by using Green Inhibitor, *2022 IOP Conf. Ser.: Mater. Sci. Eng*., 2022, **1258**, 012035. doi: 10.1088/1757-899X/1258/1/012035
15. Z. Liu, W. Yang, X. He, T. Cheng, H. Huang, J. Xiong and G. Huang, Synthesis of a green inhibitor and its inhibition behavior on AZ91D magnesium alloy in distilled water, *Surf. Interfaces*, 2022, **30**, 101870. doi: 10.1016/j.surfin.2022.101870
16. P. Li, Z. Shao, W. Fu, W. Ma, K. Yang, H. Zhou and M. Gao, Enhancing corrosion resistance of magnesium alloys via combining green chicory extracts and metal cations as organic-inorganic composite inhibitor, *Corrosion Communications*, 2023, **9**, 44–56. doi: 10.1016/j.corcom.2022.06.002
17. Y. Qian, Y. Wu, X. Guo and L. Wang, A synergistic anti-corrosion effect of longan residue extract and sodium dodecylbenzenesulfonate composition on AZ91D magnesium alloy in NaCl solution, *Corros. Eng., Sci. Technol*., 2022, **57**, 322–330. doi: 10.1080/1478422X.2022.2060788
18. V.A. Ogorodnikova, Yu.I. Kuznetsov and A.A. Chirkunov, Inhibition of Corrosion of Mg90 Alloy with Compositions Based on Sodium Oleate. Part I. Salts of Higher Alkenyl and Aryl Carboxylates, *Prot. Met. Phys. Chem. Surf*., 2021, **24**, 1336–1343. doi: 10.1134/S2070205121070121
19. V.A. Ogorodnikova, Yu.I. Kuznetsov, N.P. Andreeva, A.Y. Luchkin and A.A. Chirkunov, Adsorption of anions of higher carboxylic acids on magnesium from weakly alkaline aqueous solutions, *Russ. J. Phys. Chem. A*, 2020, **94**, 1104–1110. doi: 10.1134/S0036024420060187
20. V. Upadhyay, Z. Bergseth, B. Kelly and D. Battocchi, Silica-Based Sol-Gel Coating on Magnesium Alloy with Green Inhibitors, *Coatings*, 2017, **7**, 86. doi: 10.3390/coatings7070086
21. K.R. Ansari, A. Singh, A.K. Alanazi and M.A. Quraishi. CHAPTER 9 - Vapor inhibitors for corrosion protection. Editor(s): Lei Guo, Chandrabhan Verma, Dawei Zhang, *Eco-Friendly Corrosion Inhibitors*, 2022, 127–136. doi: 10.1016/B978-0-323-91176-4.00012-X
22. Yu.I. Kuznetsov, N.N. Andreev and A.I. Marshakov, Physicochemical Aspects of Metal Corrosion Inhibition, *Russ. J. Phys. Chem*., 2020, **94**, 505–515. doi: 10.1134/S0036024420030152

23. F.A. Ansari, C. Verma, Y.S. Siddiqui, E.E. Ebenso and M.A. Quraishi, Volatile corrosion inhibitors for ferrous and non-ferrous metals and alloys: A review, *Int. J. Corros. Scale Inhib*., 2018, **7**, 126–150. doi: 10.17675/2305-6894-2018-7-2-2
24. O.A. Goncharova, A.Yu. Luchkin, I.N. Senchikhin, Yu.B. Makarychev, V.A. Luchkina, O.V. Dement'eva, S.S. Vesely and N.N. Andreev, Structuring of Surface Films Formed on Magnesium in Hot Chlorobenzotriazole Vapors, *Materials*, 2022, **15**, 6625. doi: 10.3390/ma15196625
25. O.A. Goncharova, A.Y. Luchkin, I.A. Archipushkin, N.N. Andreev, Yu.I. Kuznetsov and S.S. Vesely, Vapor-phase protection of steel by inhibitors based on salts of higher carboxylic acids, *Int. J. Corros. Scale Inhib*., 2019, **8**, 568–599. doi: 10.17675/2305-6894-2019-8-3-9
26. A.A. Chirkunov, A.G. Rakoch, E.P. Monakhova, A.A. Gladkova, Z.V. Khabibullina, V.A. Ogorodnikova, M. Serdechnova, C. Blawert, Yu.I. Kuznetsov and M.L. Zheludkevich, Corrosion protection of magnesium alloy by PEO-coatings containing sodium oleate, *Int. J. Corros. Scale Inhib*., 2019, **8**, 1170–1188. doi: 10.17675/2305-6894-2019-8-4-22
27. GOST 804-94, *Magnesium in ingots. Technical specifications* (in Russian).
28. *ELLIPSHEET: Spreadsheet Ellipsometry (Excel Ellipsometer)*, Link
29. N. Mahato and M.M. Singh, Investigation of passive film properties and pittinp resistance of ALSI 316 in aqueous ethanoic acid containing chloride ions using electrochemical impedance spectroscopy (EIS), *Port. Electrochim. Acta*, 2011, **29**, 233–251. doi: 10.4152/pea.201104233
30. J.R. Macdonald and E. Barsoukov, *Impedance Spectroscopy: Theory, Experiment, and Applications*, John Wiley and Sons, Inc.: Hoboken, NJ, USA, 2005, 1–13. doi: 10.1002/0471716243
31. A.Yu. Luchkin, O.A. Goncharova, I.A. Arkhipushkin, N.N. Andreev and Yu.I. Kuznetsov, The effect of oxide and adsorption layers formed in 5-Chlorobenzotriazole vapors on the corrosion resistance of copper, *J. Taiwan Inst. Chem. Eng*., 2020, **117**, 231–241. doi: 10.1016/j.jtice.2020.12.005
32. O.A. Goncharova, A.Yu. Luchkin, N.P. Andreeva, V.E. Kasatkin, S.S. Vesely, N.N. Andreev, Yu.I. Kuznetsov, Mutual effect of components of protective films applied on copper and brass from octadecylamine and 1,2,3-benzotriazole vapors, *Materials*, 2022, **15**, 1541. doi: 10.3390/ma15041541

♦ ♦ ♦